Discrete Model-Predictive-Control-Based Maximum Power Point Tracking for PV Systems: Overview and Evaluation

Abderezak Lashab, *Student Member, IEEE*, Dezso Sera, *Senior Member, IEEE*, Josep M. Guerrero, *Fellow, IEEE*, Laszlo Mathe, *Senior Member, IEEE*, and Aissa Bouzid

***Abstract*—The main objective of this work is to provide an overview and evaluation of discrete model-predictive control (MPC)-based maximum power point tracking (MPPT) for photovoltaic systems. A large number of MPC-based MPPT methods have been recently introduced in the literature with very promising performance; however, an in-depth investigation and comparison of these methods has not been carried out yet. Therefore, this paper has set out to provide an in-depth analysis and evaluation of MPC-based MPPT methods applied to various common power converter topologies. The performance of MPC-based MPPT is directly linked with the converter topology, and it is also affected by the accurate determination of the converter parameters; sensitivity to converter parameter variations is also investigated. The static and dynamic performance of the trackers is assessed according to the EN 50530 standard, using detailed simulation models, and validated by experimental tests. The analysis in this work aims to present useful insight for practicing engineers and academic researchers when selecting the maximum power point tracker for their application.**

***Index Terms*—Boost, EN 50530, flyback, grid connected, maximum power point tracking (MPPT), model-predictive control (MPC), photovoltaic (PV), Z-source inverter (ZSI).**

I. Introduction

PHOTOVOLTAIC (PV) systems are one among the fastest growing renewable energy generation technologies. Around half a million PV panels were installed every day all over the world in 2015 [1]. By 2050, the cumulative installed capacity of PV systems could reach 3000 GW, providing 4500 TWh per year, i.e., around 11% of global electricity production [2]. Concerning the price, from 2009 to 2016, the cost of PV modules has been reduced by five times and the cost of full PV systems has been reduced by almost three times [2].

Manuscript received June 1, 2017; revised July 31, 2017 and September 11, 2017; accepted October 10, 2017. Date of publication October 17, 2017; date of current version April 20, 2018. Recommended for publication by Associate Editor T. Suntio. *(Corresponding author: Abderezak Lashab.)*

A. Lashab and A. Bouzid are with the Laboratoire d'Electrotechnique de Constantine, Université des Frère Mentouri, 25000 Constantine, Algeria (e-mail: Abderezak.lashab@lec-umc.org; you.bouzid@yahoo.fr).

D. Sera, J. M. Guerrero, and L. Mathe are with the Department of Energy Technology, Aalborg University 9220 Aalborg, Denmark (e-mail: des@et.aau.dk; joz@et.aau.dk; lam@et.aau.dk).

Color versions of one or more of the figures in this paper are available online at http://ieeexplore.ieee.org.

Digital Object Identifier 10.1109/TPEL.2017.2764321

The output power characteristic of the PV module is nonlinear, and it depends on the meteorological conditions, such as solar irradiance and temperature. Usually, there is one operating point where the PV panel generates its maximum power. Also, the PV system efficiency can be degraded if the PV panel is not forced to operate at its maximum power at all times regardless of the environmental conditions [3]. Hence, a means that makes the PV module operate at its maximum power is required. Usually, a dc–dc or dc–ac converter is employed with an algorithm that controls this later; this algorithm is called the maximum power point tracker. The most well-known maximum power point tracking (MPPT) algorithm is the Perturb and Observe (P&O) [4]–[6], but this algorithm does not converge to the true maximum power point (MPP) [7], [8], and there occurs some oscillations around the MPP [9]. The incremental conductance (INC) method [10]–[12] was considered as an improved P&O method, until Sera *et al.* [4] proved that P&O and INC have equivalent performance. The step size in these two methods is defined by the conditions of the steady-state calculation accuracy and the dynamic response time, which is a tradeoff [13]. Other classical methods are also reported in the literature, such as fractional short-circuit current and fractional open-circuit voltage [14], but these methods also do not converge to the true MPP.

In the last few years, intelligent methods such as fuzzy logic [15], neural network [16], and model predictive control (MPC) [3] have been developed for better extraction of the maximum power from the PV arrays. The application of MPC on power electronics has started more than 20 years ago, but this was only for low switching frequency due to the limitations of microprocessors at that time [17]. In the last decade, the application of MPC in power electronics has increased considerably with the development of multitask and high-frequency microprocessors [18]–[21]. The MPC methods used in power electronics are classified into two main classes [18], [22]: the first one is continuous-control-set MPC (CCS-MPC) and the second is finite-control-set MPC (FSC-MPC, hereafter referred to as FMPC), also known as discrete MPC. In CCS-MPC, the continuous output of the predictive controller is used for the generation of the switching state by employing a modulator, whereas the optimization in FMPC is done by using the discrete-time model of the system for the available switching states of the power

TABLE I
REPORTED EFFICIENCIES (%) OF MPC-MPPT USING DIFFERENT CONVERTERS UNDER VARIOUS CONSTANT IRRADIANCE LEVELS

Power Converter Type	MPC-MPPT Type	Solar irradiance				Average Efficiency
		1000 W/m^2	750 W/m^2	500 W/m^2	250 W/m^2	
Flyback [7]	FMPC-MPPT (P&O)	99.60	99.95	99.71	99.70	99.74
Z-Source inverter [3]	DMPC- MPPT	99.24	99.07	99.68	99.58	99.39
Boost [38]	Oriented Voltage and Current	No Data provided				
Multilevel Boost [45]	FMPC-MPPT (P&O)	No Data provided				
Sensorless Flyback [42]	FMPC-MPPT (INC)	99.35	99.45	99.95	99.90	99.66
Boost [34] (simulation)	FMPC-MPPT (INC)	No Data provided				99.86

converter, and the appropriate switching state will be applied in the next sampling period. FMPC offers the advantages of being easy to implement and applicable on nonlinear systems [23], but its application on nonlinear systems is still limited by the dynamics of the system, contrary to CCS-MPC [24]. Recently, both MPC classes, CCS-MPC such as presented in [24] and [25] and FMPC [3], [26], have been used for tracking the MPP of the PV strings on the basis that they offer fast tracking during transient state and low power oscillations in the steady state compared with the classical methods.

MPC techniques provide a fast dynamic response with relatively high stability margin compared to classical control schemes, which make them more suited for MPPT of PV systems operating under fast changing atmospheric conditions [27]. However, there are still several open instability problems. Generally, it is the case when the operating point is not in the neighborhood of the tracked reference [28]. In [29], the authors proposed the Lyapunov function for setting the cost function parameters based on Lyapunov stability theory to overcome this problem in power electronics generally. This solution can be used also on MPPT, since it is not a particular case. The FMPC algorithm for power electronic converters is summarized in the following steps [30]: measure the currents and the voltages, predict the currents and the voltages for the next sampling time, evaluate the cost functions, select the switching states according to the minimized cost function, and, finally, apply the selected switching states to the converter.

Concerning MPPTs, the cost function is calculated based on the predicted PV currents and/or the predicted PV voltages for all the switching states and the current and/or voltage reference. These references are usually calculated using the P&O method such as in [26] and [31] or INC as in [32] and [33]. Eventually, the switching states corresponding to the reduced cost function will be applied. The application of MPC on MPPT in these papers is almost the same; the only difference is the converter topology: in [32], it has been applied on a switched inductor quadratic boost converter, in [34] on a boost converter, in [26] on a flyback converter, in [31] on a high-gain multilevel dc–dc converter (multilevel boost converter), in [33] on a grid-tied multilevel boost converter, in [35] on an ultra-step-up boost converter, and in [36] on a submultilevel inverter. However, in [3], [37], and [38], MPC on MPPT has been applied otherwise. In [3] and [37], the predicted voltages and currents for only two states have been calculated: the first state for voltage reference larger than the PV voltage and the second state for voltage reference smaller than the PV voltage. In the following, the PV currents using a digital observer (DO) corresponding to these two voltage states are calculated. At the end, the voltage corresponding to the largest predicted power is chosen as a reference. The only difference between these two is that, in [3], MPC has been applied on Z-Source inverter (ZSI), while in [37], the boost converter is the target application. In [38], the proposed voltage-oriented MPPT by Kadri *et al.* [39] has been improved to current- and voltage-oriented MPPT using MPC, where the used topology was a boost converter. Note that, in all these proposed schemes, the prediction of the PV current and voltage is performed within a static PV curve for the actions that could be made on the duty cycle of the gating signal.

In the literature, it has been reported that the application of the MPC method on MPPTs compared to classical methods offers the following key advantages: robust control [36], a higher convergence speed under a changing environmental conditions [26], and less ripple during the steady state [38]. However, as shown later in this paper, the experimental results do not confirm this statement, showing that the DO-based MPC in fact produces higher ripple than P&O under low irradiance. Another important advantage of FMPC compared to the classical methods is the application of the switching states directly from the control without using a modulation stage and without using a proportional–integral (PI) controller [18]. This latter requires relatively a long time for the system to attain steady-state operation. Also, increasing the response time between two successive reference outputs deteriorates the dynamic performance [40]. However, as found in the literature, the MPC method has three disadvantages. The first disadvantage is that it requires a microprocessor with high frequency, and that it needs a small sampling time (Ts). The largest sampling time found in the literature is about 75 μs, which is reached by a calculation effort minimization algorithm done in [41]. The second one is that in some converters, it needs more than one voltage sensor and/or more than one current sensor, for example, in [33], the authors used one current sensor and two voltage sensors. Also, the model parameter mismatch is another disadvantage, which influences the MPPT efficiency negatively, as discussed and investigated in [3] and [42].

Tables I and II show the reported efficiencies of MPC-MPPT by using different converter topologies under various constant irradiance levels and with model parameter mismatch. The efficiency of the MPPT can be improved enormously, by either improving the MPPT algorithm or the power converter [43].

TABLE II
REPORTED EFFICIENCIES (%) OF MPC-MPPT USING DIFFERENT CONVERTERS WITH MODEL PARAMETER MISMATCH

Power Converter Type	MPC-MPPT Type	Parameters Mismatch					Average Efficiency
		–30%	–15%	0%	+15%	+30%	
Flyback [7]	FMPC-MPPT (P&O)	No Data provided					
Z-Source inverter [3]	DMPC-MPPT	98.30	99.00	99.25	99.20	98.90	98.93
Boost [38]	Oriented Voltage and Current	No Data provided					
Multilevel Boost [45]	FMPC-MPPT (P&O)	No Data provided					
Sensorless Flyback [42]	FMPC-MPPT (INC)	99.15	99.85	99.95	99.85	99.45	99.65
Boost [34]	FMPC-MPPT (INC)	No Data provided					

Also, the used PV simulator plays an important role in the assessment of the MPPT efficiency. Some PV simulators have some difficulties in adjusting the operating point compared to others, such as in [44]. Based on this, the results in these tables cannot be compared to each other in terms of control strategy. A detailed and thorough comparison of these proposed methods has not been carried out yet. In this regard, this paper has set out for a detailed and fair comparison of these methods by implementing them on the same test setup, under the same power range, and with the same updating rate.

The DO-based MPC-MPPT (DMPC-MPPT) operation principle is also based on the discrete-time model and the cost function minimization; therefore, it can be classified into discrete MPC-MPPT as well. This class is the one described and analyzed in this paper. The choice of this class has been made on the basis that it is the most relevant, cited, and published compared to other predictive control MPPTs.

This paper is organized in the following way. Section II shows the operational principles of both FMPC-MPPT and DMPC-MPPT. Section III presents examples of discrete MPC on a number of power converter topologies. Section IV explains in detail the simulation environment, experimental setup, and the test conditions. Section V shows the simulation and experimental results followed by a discussion. In Section VI, a conclusion of this work is presented.

II. MPC-BASED MPPT

Predictive control denotes to a vast class of controllers, which has been used in power electronics. All these controllers have been used for pursuing the MPP as well [3], [7], [42], [46]–[49]. In this paper, we propose that these controllers are classified into four major types as sketched in Fig. 1. The trajectory-based control action is performed by making the controlled variable track a predefined trajectory. In deadbeat control, the error is forced to be zero for the next sampling instant by the optimal actuation. The feature of hysteresis-based MPPT is to maintain the controlled variable within the barriers of a hysteresis area. The optimization criterion is based on the minimization of a cost function in both continuous and discrete MPC-MPPT. Continuous MPC-MPPT is based on the continuous-time model, where the prediction model is elaborated using the Taylor series expansion. Discrete MPC-MPPT is explained in detail in the following subsections.

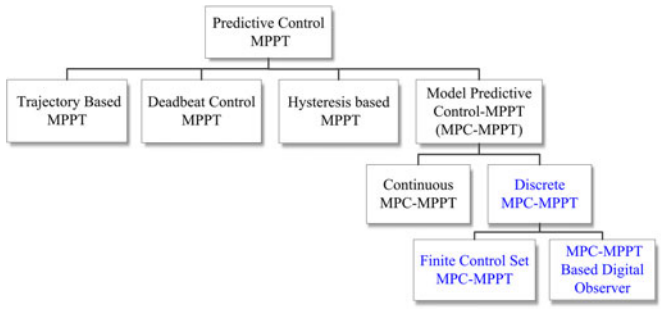

Fig. 1. Classification of predictive-control-based MPPT methods.

A. FMPC-Based MPPT

FMPC has been used as a very powerful method to control the electrical energy employing power converters [50]. FMPC is easy to apply and has the ability to predict the behavior of the controlled variable by N horizon length ahead, even in the existence of nonlinearities. In addition, it can avoid the use of PI controllers and the whole modulation stage. The horizon length N is the prediction length as a function of the sample time. In general, using a larger horizon length for the implementation of FMPC produces better performance [22] and subsequently more accurate tracking of the provided reference (MPP). However, the computation complexity increases exponentially with the increase of the horizon length. This increase imposes the designer to trade off online computational effort versus MPP tracking performance. Generally, FMPC provides excellent performance by using small values of the horizon length. In this paper, the horizon length $N = 1$, which means the predictions are done by *one* sample time ahead as shown in Fig. 3. The aim of using this modification on MPPT is for both to decrease the response time to achieve the MPP under variable meteorological conditions and also to operate with fewer oscillations under constant solar irradiation and temperature.

The general control block diagram of an FMPC-MPPT method and the operation principle are illustrated in Figs. 2 and 3, respectively. The first step is to measure the system variables. The second step is to calculate the predicted variables based on the extracted equations from the system and the measured data. This calculation should be for all the possible switching states (voltage vectors), as shown in Figs. 3 and 4. The next step is to minimize the cost function based on the predicted variables and their references. In a case of the MPPT system, the variables are

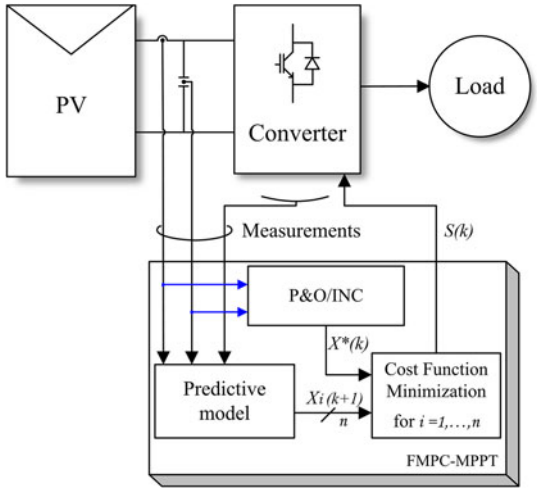

Fig. 2. General control block diagram of FMPC used for tracking the MPP.

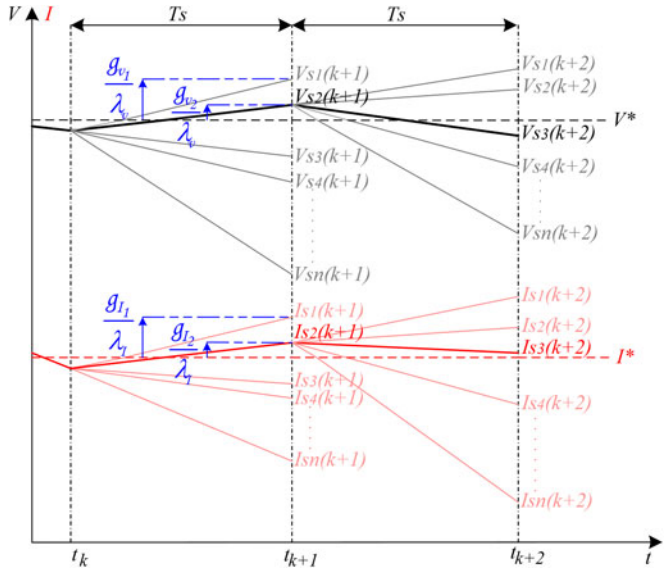

Fig. 3. Operation principle of an FMPC method on power electronics.

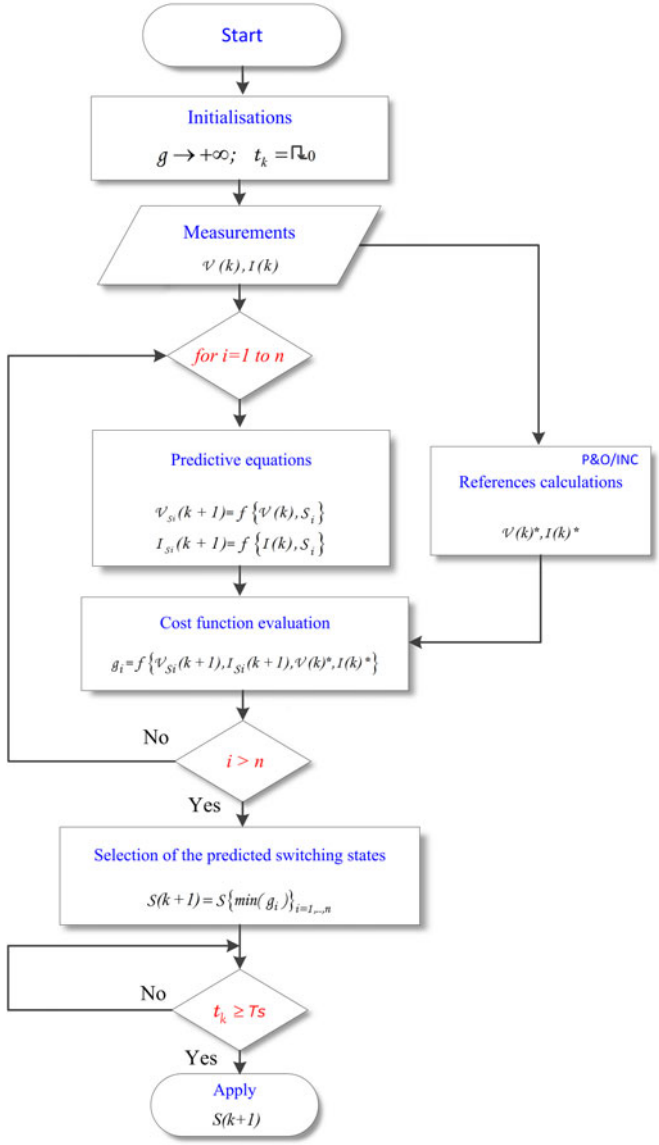

Fig. 4. Flowchart of the general finite-control-set MPC-based MPPT.

the PV current and voltage. Hence, the measurements consider the PV current $I(k)$ (k indicates the current sample time) and voltage $\mathcal{V}(k)$ and the variables that are included in the predictive equations.

The predicted variables should be the predicted PV currents $I_{Si}(k+1)$ and voltages $\mathcal{V}_{Si}(k+1)$ for all the possible voltage vectors ($k+1$ indicates the next sample time). The cost function is minimized based on these predictions and their predicted references $\mathcal{V}^*(k+1)$ and $I^*(k+1)$. Usually, the sampling time is in range of microseconds; thus, it is assumed that the predicted reference variable is equal to the instantaneous reference variable $\mathcal{X}^*(k+1) = \mathcal{X}^*(k)$ [22]. Generally, the cost function used for tracking the MPP is written as follows:

$$g_{i\{1,\ldots,n\}} = \lambda_{\mathcal{V}} \cdot \left|\mathcal{V}_{\mathrm{S}i}(k+1) - \mathcal{V}^*\right| + \lambda_I \cdot \left|I_{\mathrm{S}i}(k+1) - I^*\right| \quad (1)$$

where λ_I and $\lambda_{\mathcal{V}}$ are the weighting factors, g is the cost function, $\mathrm{S}i$ is the switching state, and n is the number of the possible switching states ($n = 8$, in a case of a classical three-phase two-level voltage-source inverter). Until now, there is no exact model for the calculation of the weighting factors [18]; indeed, they are still defined by empirical tests. The reference variables are obtained from another algorithm (For example, from P&O or INC algorithm). Since the time of executing the algorithm is less than Ts, the one before last step is to wait until the time from the previous application of the switching state (t_k) reach Ts, as shown in Fig. 4. Eventually, the application of the switching state $\mathrm{S}(k)$ corresponding to the evaluated cost function.

B. DO MPPT-Based MPC

Since DMPC employs the PV characteristic for the construction of the predictive model, it has been used only for tracking the MPP, contrary to FMPC that has been used in many applications such as motor control [51], [52], tracking the MPP in renewable energy systems, electrical power quality improvement, etc.

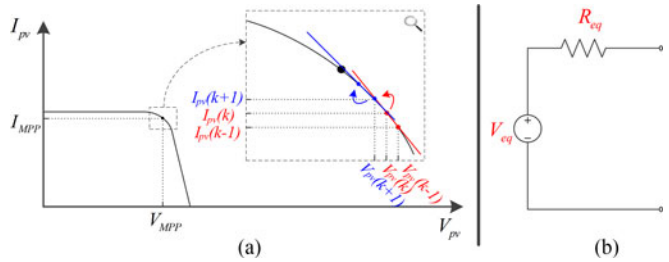

Fig. 5. (a) Extrapolation of the predicted PV current based on the predicted PV voltage and the straight line equation. (b) PV module equivalent circuit model used for the prediction of the PV string power.

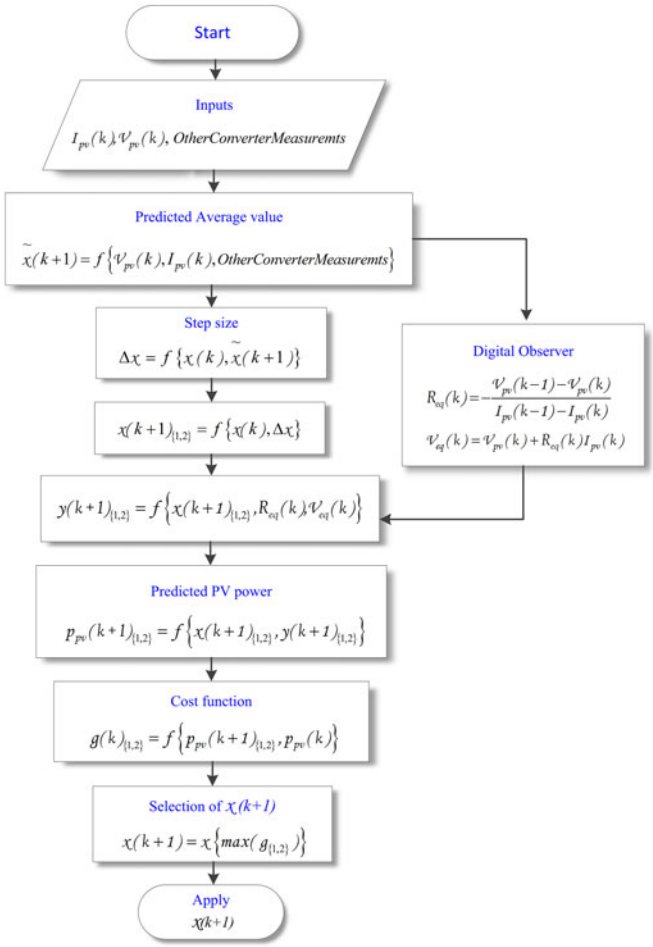

Fig. 6. Flowchart of the general DMPC-MPPT.

DMPC-MPPT tracks the MPP by sliding the PV voltage to the voltage that makes the PV string generate its maximum power (V_{MPP}). Fig. 6 shows the flowchart of the general DMPC-MPPT, such as X is the PV voltage and y is the PV current in the case of voltage control, while in the other way around for current control.

The first step is the calculation of the step size $\Delta \mathrm{X}$ (ΔV, voltage control is used in this section) by estimating the predicted average PV voltage, such as in [3]. Also, some examples of the estimation of the step size are elaborated in Section III. However, as described in [37], a fixed voltage step size could also be set.

The second step consists of the calculation of the predicted PV voltages, which are defined as the difference between the PV voltage and the step size for the first case, and the addition of the PV voltage and the step size for the second case

$$V_{\mathrm{pv}}(k+1)_{\{1,2\}} = V_{\mathrm{pv}}(k) \pm \Delta V. \tag{2}$$

The third step consists of the calculation of the predicted PV currents by means of the DO [3], [37]. The DO models the PV array as two series elements V_{eq} and R_{eq}, as shown in Fig. 5(b). The DO generates the values of these elements in order to allow the algorithm to calculate the predicted PV current corresponding to a given PV voltage. These elements are calculated based on $V_{\mathrm{pv}}(k-1)$ and $I_{\mathrm{pv}}(k-1)$, which are the PV voltage and current measured at the previous sampling time, respectively. Next, these elements will be substituted into a straight line equation (3), which is obtained by the application of Kirchoff´s voltage law on the equivalent PV module circuit

$$V_{\mathrm{eq}}(k) = V_{\mathrm{pv}}(k) + R_{\mathrm{eq}}(k) \cdot I_{\mathrm{pv}}(k) \tag{3}$$

$$R_{\mathrm{eq}}(k) = -\frac{V_{\mathrm{pv}}(k-1) - V_{\mathrm{pv}}(k)}{I_{\mathrm{pv}}(k-1) - I_{\mathrm{pv}}(k)}. \tag{4}$$

The shifting increment is small, which implies that the straight line used for the prediction is small. Hence, the predicted PV current $I_{\mathrm{pv}}(k+1)$ interpolated by this straight line equation will be on the PV curve, as shown in Fig. 5(a).

The fourth step is the evaluation of the cost function, which is described as the difference between the predicted PV power "$P_{\mathrm{pv}}(k+1)_{\{1,2\}} = V_{\mathrm{pv}}(k+1)_{\{1,2\}}.I_{\mathrm{pv}}(k+1)_{\{1,2\}}$" and the PV power at the present sampling instant, which can be written in the following form:

$$g_{\{1,2\}} = P_{\mathrm{pv}}(k+1)_{\{1,2\}} - P_{\mathrm{pv}}(k). \tag{5}$$

Finally, the application of the predicted PV voltage $V_{\mathrm{pv}}(k+1)$ corresponds to the chosen cost function. Hence, contrary to FMPC, a PI controller and a modulation stage are required in this method.

III. Examples of Discrete MPC-MPPT Based on Some Power Converter Topologies

In order to give a comprehensive concept of discrete MPC-MPPT methods already described in the previous section, and since the application of FMPC-MPPT and DMPC-MPPT is substantially related to the converter topology, this section has been devoted to the presentation of some examples of these methods on some power converter topologies.

A. DC–DC Boost Converter

1) FMPC-MPPT Based on a Boost Converter: A flowchart of FMPC-MPPT used to control the boost converter can be performed by following the procedure of the flowchart presented in Fig. 4, where the aim of this control is to withdraw the maximum power from the PV array under any environmental conditions. The first step of the FMPC-MPPT application procedure is the

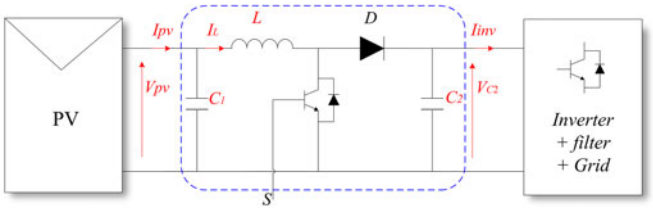

Fig. 7. Simplified schematic of the overall grid-connected PV system configuration using dc–dc boost converter for withdrawing the maximum power.

extraction of the system equations. By applying Kirchoff's voltage law on Fig. 7, the continuous-time expressions of the boost converter for the two states can be found as follows:

$$\begin{cases} L\frac{dI_L}{dt} = V_{\text{pv}} \\ C_2\frac{dV_{C2}}{dt} = -I_{\text{inv}}, \end{cases} \quad \text{for } S = 1 \tag{6}$$

and

$$\begin{cases} L\frac{dI_L}{dt} = V_{\text{pv}} + V_{C2} \\ C_2\frac{dV_{C2}}{dt} = I_{\text{pv}} - I_{\text{inv}}, \end{cases} \quad \text{for } S = 0 \tag{7}$$

where $S = 1$ and $S = 0$ denote *switch* ON and *switch* OFF states, respectively. Generally, the discrete-time model is obtained by using Euler´s forward-difference law, which can be written as

$$\frac{dx}{dt} \approx \frac{x(k+1) - x(k)}{Ts}. \tag{8}$$

The application of Euler's law on the boost *switch* ON equations yields

$$\begin{cases} I_L(k+1) = \frac{Ts}{L}V_{\text{pv}}(k) + I_L(k) \\ V_{C2}(k+1) = -\frac{Ts}{C_2}I_{\text{inv}}(k) + V_{C2}(k). \end{cases} \tag{9}$$

The discrete-time model of the boost during the *switch* OFF state was found similarly as

$$\begin{cases} I_L(k+1) = \frac{Ts}{L}\left(V_{\text{pv}}(k) + V_{C2}(k)\right) + I_L(k) \\ V_{C2}(k+1) = \frac{Ts}{C_2}\left(I_{\text{pv}}(k) - I_{\text{inv}}(k)\right) + V_{C2}(k). \end{cases} \tag{10}$$

The average value of the current through the capacitor C_1 is zero. Thus, the average current through the inductor L is equal to the average value of the PV current. Therefore, the estimated value of the PV current in the next sampling time can be expressed based on (9) and (10).

Based on the fact that

$$V_{\text{pv}}(k+1) = (1-D)\cdot V_{C2}(k+1) \tag{11}$$

the predicted PV voltages can be obtained by using (9) and (10). D is the duty ratio. Now, the cost function can be minimized using the following equation based on these predicted variables and their references:

$$g_{\{0,1\}} = \lambda_I \cdot \left|I_L(k+1)_{\{0,1\}} - I^*\right| + \lambda_v \cdot \left|V_{\text{pv}}(k+1)_{\{0,1\}} - V^*\right|. \tag{12}$$

The one before last step is to wait until t_k reaches Ts. At that moment, the switching state corresponding to the minimized cost function is ready to be applied directly to the converter.

2) DO MPC-MPPT Based on a Boost Converter: Fig. 6 illustrates the flowchart of the DMPC-MPPT algorithm that can be used to control the boost converter. This control is performed by using the aforementioned steps. In this subsection, current control is used, and the current increment is chosen to be variable. This latter is described as the absolute difference between the average predicted PV current and the instantaneous PV current, which can be written as follows:

$$\Delta I = \left|\tilde{I}_L(k+1) - I_{\text{pv}}(k)\right|. \tag{13}$$

The average predicted PV current is calculated by using the predicted current through the inductor in both cases, *switch* ON (9) and *switch* OFF (10), multiplied by the switching state:

$$\tilde{I}_L(k+1) = I_{L1}(k+1)\cdot S(k) + I_{L0}(k+1)\cdot(1 - S(k)). \tag{14}$$

Once the predicted PV currents "$I_{\text{pv}}(k+1)_{\{1,2\}} = I_{\text{pv}}(k) \pm \Delta I$" are calculated, the DO will determine the predicted PV voltages, and the cost function can be calculated based on these predictions using (5). A PI controller is used to minimize the error between the predicted PV voltage matching the evaluated cost function and the PV voltage at the current sampling period. Then, the output of this controller is used to generate the pulses for the control of the boost converter through a modulator.

B. Z-Source Inverter

The ZSI has been introduced in 2003 [53]. Since then, the family of ZSIs has been used in a wide range of power conversion as an interface between different types of sources and loads (dc–dc, ac–dc, dc–ac, and ac–ac). Contrary to the classical inverter, among its characteristics, is that it has a wide range of output voltage; in fact, it can step up and step down the output voltage. In addition, the upper and lower power switches of each leg can be triggered simultaneously without any risk of damage [53]. This latter case is named as shoot-through (ST) state [see Fig. 9(a)]. As found in the literature, there are three modulation strategies of the ZSI: simple-boost modulation [53], constant-boost modulation [54], and maximum-boost modulation [55]. In this paper, simple-boost modulation is used for the generation of the switching signals.

The rapport between the ac-side voltage and the PV-side voltage is shown as follows:

$$M.B = \frac{\hat{V}_{\text{inv}}}{V_{\text{pv}}} = B_B \tag{15}$$

where B_B is the buck-boost factor, M is the modulation index, $\hat{V}_{\text{inv}}$ is the ac-side peak voltage, and B is the boosting factor. Being D_{ST} the ST duty ratio, the relation between the boosting factor and the modulation index can be expressed in the following form:

$$B = \frac{1}{2 - 1/M} = \frac{1}{1 - 2D_{\text{ST}}}. \tag{16}$$

1) FMPC-MPPT Based on the ZSI: The determination of the cost function is a key part of the MPC scheme, since it is defined by the variables that need to be controlled. In a single-stage grid-connected PV system, one of the controlled variables

is the current injected to the grid, which must be in phase and has the same frequency as the grid voltage. Moreover, the total harmonic distortion of the current should respect the values prescribed by the IEEE 519 Standards. The second variable is the PV string voltage that should be shifted to the target voltage at which the PV panel should work at its maximum power, whatever the meteorological conditions are present. Therefore, the cost function can be defined as follows:

$$g_i = \lambda_I \left| I_{L1_i}(k+1) - I^* \right| + \lambda_v \left| V_{\mathrm{pv}_i}(k+1) - V^* \right| + \lambda_{\mathcal{G}} \left| I_{\mathcal{G}i}(k+1) - I_{\mathcal{G}}{}^* \right| \tag{17}$$

where $I_{L1}(k+1)$ and $V_{C1}(k+1)$ are the predicted current through the inductor L_1 and the predicted voltage at the terminals of the capacitor C_1, respectively. The relationship between $V_{C1}(k+1)$ and the predicted PV voltage is as follows:

$$V_{\mathrm{pv}_i}(k+1) = \frac{2}{1+B} V_{C1i}(k+1). \tag{18}$$

The purpose of including $I_{L1}(k+1)$ and $V_{C1}(k+1)$ in the cost function is to shift the PV voltage to V_{MPP}. $I_{\mathcal{G}}(k+1)$ is the predicted current injected to the grid, which is used in the cost function to fulfill the conditions of the injected current based on a given grid current $I_{\mathcal{G}}^*$ (see Fig. 3). In order to define the predicted variables in the first and second terms of the cost function, the model of the ZSI in the discrete-time domain is needed. During the non-ST state, the discretized equations of the ZSI are as follows [3]:

$$\begin{cases} I_{L1}(k+1) = I_{L1}(k) + \frac{Ts}{L_1}(V_{\mathrm{pv}}(k) - V_{C1}(k) - R_{L1} I_{L1}(k)) \\ V_{C1}(k+1) = V_{C1}(k) + \frac{Ts}{C_1}(I_{L1}(k+1) - I_{\mathrm{inv}}(k+1)) \end{cases} \tag{19}$$

whereas during the ST state, the discrete-time model is formulated as

$$\begin{cases} I_{L1}(k+1) = I_{L1}(k) + \frac{Ts}{L_1}(V_{C1}(k) - R_{L1} I_{L1}(k)) \\ V_{C1}(k+1) = V_{C1}(k) - \frac{Ts}{C_1} I_{L1}(k+1) \end{cases} \tag{20}$$

$$I_{\mathrm{inv}}(k+1) = I_{\mathcal{G}}(k) \cdot (S_a(k) - S_b(k)) \tag{21}$$

where $S_a(k)$ and $S_b(k)$ are the instantaneous switching states, R_{L1} is the internal resistance of the inductor L_1, and $I_{\mathrm{inv}}(k+1)$ is the current going through the inverter in the next sampling period. In order to calculate the predicted variable in the third term of the cost function, the output inverter voltage V_{inv} as a function of its current and filter parameters should be defined. The application of Kirchoff´s law on the ac side of the system (see Fig. 8) provides the following vector differential expression:

$$V_{\mathrm{inv}} = L_f \frac{dI_{\mathcal{G}}}{dt} + R_f I_{\mathcal{G}} + V_{\mathcal{G}}. \tag{22}$$

The substitution of Euler's law into (22) gives the following discretized equation:

$$I_{\mathcal{G}}(k+1) = \left(1 - \frac{R_f}{L_f} Ts\right) I_{\mathcal{G}}(k) + \left(V_{\mathrm{inv}}(k+1) - V_{\mathcal{G}}(k)\right) \frac{Ts}{L_f} \tag{23}$$

where $V_{\mathrm{inv}}(k+1)$ is the inverter voltage vector in the next sampling instant, which can be defined as a function of the switching states as follows:

$$V_{\mathrm{inv}}(k+1) = V_{\mathrm{pv}}(k) \cdot B_B \cdot (S_a(k) - S_b(k)). \tag{24}$$

The cost function should be calculated for all the available voltage vectors including the ST state. The combination of both the ac-side voltage vector and the PV voltage that minimizes the cost function will be applied in the next sampling cycle. This combination is based on the selected weighting factors, which require a certain sort of tradeoff among the objectives, since it may not be easy to determine which one is the optimum.

2) DO MPC-MPPT Based on the ZSI: The voltage increment in this subsection is recalculated at each sampling time. According to Fig. 6, to define the step size in the case of the ZSI, the predicted average PV voltage $\tilde{V}_{\mathrm{pv}}(k+1)$ needs to be developed. This latter is calculated using the discretized equations of the converter during the ST state (19) and the non-ST state (20). By substituting (18) into (19) and (20), the average predicted PV voltage can be written as

$$\tilde{V}_{\mathrm{pv}}(k+1) = \frac{2}{1+B}\left(\left(V_{C1}(k) + \frac{Ts}{C_1}(I_{L1}(k+1) - I_{\mathrm{inv}}(k+1))\right) \cdot (1 - D_{\mathrm{ST}}) + \left(V_{C1}(k) - \frac{Ts}{C_1} I_{L1}(k)\right) \cdot D_{\mathrm{ST}}\right). \tag{25}$$

The voltage increment is defined as the difference between the current PV voltage and the predicted average PV voltage as follows:

$$\Delta V = \left| \tilde{V}_{\mathrm{pv}}(k+1) - V_{\mathrm{pv}}(k) \right|. \tag{26}$$

The next step of the DMPC-MPPT algorithm is the calculation of the predicted PV voltages $V_{\mathrm{pv}}(k+1)_1$ and $V_{\mathrm{pv}}(k+1)_2$ by using (2). The predicted PV currents $I_{\mathrm{pv}}(k+1)_1$ and $I_{\mathrm{pv}}(k+1)_2$ can be calculated based on the predicted PV voltages using the

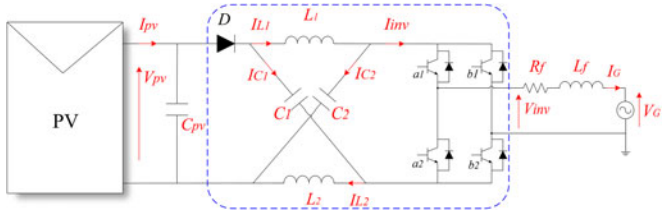

Fig. 8. Simplified schematic of the overall grid-connected PV system configuration using a Z-source inverter.

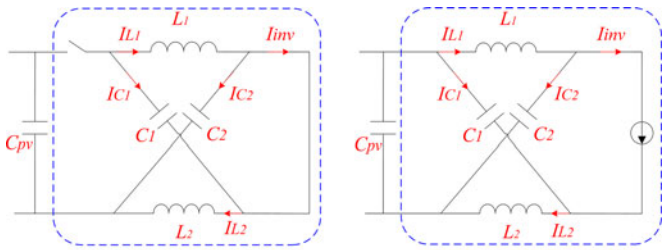

Fig. 9. (a) ZSI equivalent circuit in an ST state. (b) ZSI equivalent circuit in a non-ST state.

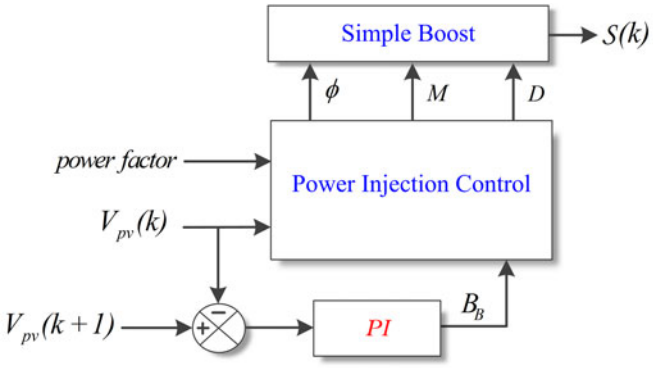

Fig. 10. Overall procedure of defining the switching state based on the predicted PV voltage and the desired power factor.

DO. Hence, all the unknown variables of the cost function (5) are ready to be substituted, and the predicted PV voltage will be set based on the evaluated cost function as shown in Fig. 6. In this subsection, it can be noted that the MPC is used only for tracking the MPP by defining the behavior of the PV power in the next sampling time $P_{\text{pv}}(k+1)$. The power injection control is done separately by using classical methods. Fig. 10 describes the overall procedure of defining the switching state based on the predicted PV voltage that needs to be applied at the next sampling time and the desired power factor, where D_{ST} and M are expressed as follows [54], [55]:

$$\begin{cases} D_{\text{ST}} = 0, & M = B_B, \quad \text{for } B_B \leq 1 \\ D_{\text{ST}} = 1 - M, & M = \frac{B_B}{2 \cdot B_B - 1}, \quad \text{for } B_B > 1. \end{cases} \tag{27}$$

C. Flyback Converter

Flyback is the third converter used in this paper as an example and for the evaluation of discrete MPC-MPPT. This latter has been already applied on the flyback converter using FMPC-MPPT [26], but it has not been thoroughly investigated. In the next two subsections, both FMPC-MPPT and DMPC-MPPT using a flyback converter are described.

1) FMPC-MPPT Based on the Flyback Converter: In a double-stage grid-connected PV system, the tracking of the MPP is done apart by employing a dc–dc converter. Hence, the static cost function (1) can be used in this subsection directly without any additional terms. In multiobjective control systems, and for more efficient reference tracking, other works proposed the use of a dynamic cost function, in which the weighting factors are optimized online [56]. With simplicity, MPC depends on the mathematical model of the variables that need to be predicted for each converter's possible operation state. The following equations can be obtained by the application of Euler's forward law on the dynamic model of the flyback converter (see Fig. 11):

$$\begin{cases} I_{\text{pv}}(k+1) = I_{\text{pv}}(k) + \frac{Ts}{Lm} V_{\text{pv}}(k) \\ V_C(k+1) = V_C(k) + \frac{Ts}{C} I_{\text{inv}}(k), \end{cases} \quad \text{for} \quad S = 1 \tag{28}$$

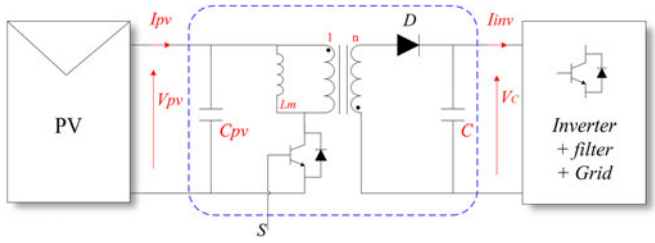

Fig. 11. Simplified schematic of the overall grid-connected PV system configuration using a flyback converter as an interface for tracking the MPP.

and:

$$\begin{cases} I_{\text{pv}}(k+1) = I_{\text{pv}}(k) - \frac{Ts}{Lm.n} V_C(k) \\ V_C(k+1) = V_C(k) + \frac{Ts}{C} \left(\frac{1}{n} I_{\text{pv}}(k) - I_{\text{inv}}(k) \right), \end{cases} \quad \text{for} \quad S = 0 \tag{29}$$

where the relationship between the output voltage of the flyback converter and the PV voltage is given by

$$V_{\text{pv}}(k+1) = V_C(k+1) \frac{1-D}{n \cdot D}. \tag{30}$$

Equations (28) and (29) are substituted into the cost function (1), and the switching action corresponding to the nearest predicted current/voltage to the current/voltage reference will be applied to the converter. A new switching state can be applied at every update instant and is maintained all along the update period. At the end of each updating period, the FMPC algorithm starts again, resulting in that named as *receding horizon.*

2) DO MPC-MPPT Based on the Flyback Converter: By using the predicted variables in both cases, switch ON and switch OFF, the average predicted voltage $\tilde{V}_{\text{pv}}(k+1)$ can be assessed, which is deduced as a function of the predicted PV voltage for the two operation states and the switching state at the current sampling cycle [57]

$$\tilde{V}_{\text{pv}}(k+1) = \frac{1-D}{n \cdot D} \left(\left(V_C(k) + \frac{Ts}{C} I_{\text{inv}}(k) \right) S(k) + \left(V_C(k) + \frac{Ts}{C} \left(\frac{1}{n} I_{\text{pv}}(k) - I_{\text{inv}}(k) \right) \right) (1 - S(k)) \right). \tag{31}$$

The predicted PV voltages $V_{\text{pv}}(k+1)_1$ and $V_{\text{pv}}(k+1)_2$ and the voltage step size can be calculated based on (2) and (26), respectively. The DO is used in this subsection for the calculation of the predicted PV currents $I_{\text{pv}}(k+1)_1$ and $I_{\text{pv}}(k+1)_2$ corresponding to the calculated predicted PV voltages. The cost function (5) will be calculated based on the predicted PV powers $P_{\text{pv}}(k+1)_1$ and $P_{\text{pv}}(k+1)_2$ and the PV power at the current sampling instant $P_{\text{pv}}(k)$. If g_1 is greater than g_2, then $V_{\text{pv}}(k+1)_1$ will be chosen as the next PV voltage; otherwise, $V_{\text{pv}}(k+1)_2$ will be chosen as the next PV voltage, as depicted in Fig. 6. And this, in order to choose the predicted PV voltage that leads to a greater power harvesting form the PV string in each sampling cycle. All that remains is the control of the PV voltage on the chosen predicted PV voltage $V_{\text{pv}}(k+1)$ by using a classical voltage regulation loop, in which a PI controller is employed.

IV. System Description

To verify the theoretical analysis and to evaluate both FMPC-MPPT and DMPC-MPPT methods, simulation models have been built with the configurations shown in Figs. 7, 8, and 11. These ideal simulations were validated further by an experimental implementation of the configuration illustrated in Fig. 7.

A. Description of the Simulation Environment

The dynamic simulation was done by using a developed mathematical model of the PV array and the data sheet of the TOTAL ENERGY TE 600 PV module to emulate the behavior of a real PV string. To simulate the configurations in Figs. 7 and 11, accurate models of the boost and flyback converters have been employed for withdrawing the maximum power from the emulated PV strings and injecting it to the grid through a single-phase inverter and an *LCL* filter, where the total string voltage was set to $V_{\mathrm{MPP}} = 300\,\mathrm{V}$ and the power to $P_{\mathrm{MPP}} = 704\,\mathrm{W}$ under the standard meteorological conditions (STC, 1000 W/m^2 of solar irradiance and 25 °C of temperature). Also, the configuration in Fig. 8 has been simulated by connecting the ZSI to a PV string of $V_{\mathrm{MPP}} = 450\,\mathrm{V}$ and $P_{\mathrm{MPP}} = 1350\,\mathrm{W}$. The MPPT used for providing the references in the case of implementing FMPC-MPPT is the P&O method. With a voltage increment of $\Delta V = 1\,\mathrm{V}$ for the voltage reference and a current step size of $\Delta I = 0.025\,\mathrm{A}$ for the current reference, the sampling time and the MPPT frequency were adjusted to 50 μs and 40 Hz, respectively.

B. Description of the Experimental Setup

Fig. 12 shows the block scheme of the experimental setup, which considers the realization of the configuration shown in Fig. 7 in the case of a standalone system, where the used components were an Agilent E4360A PV simulator with two channels, each channel provides up to 600-W power (120-V, 5.1-A), a 400-W prototype dc–dc boost converter, which has been made to extract the local maximum power of a real PV panel, and a resistive load. The PV simulator emulates the uploaded $I - V$ curve of a PV string with $P_{\mathrm{MPP}} = 122\,\mathrm{W}$ at $V_{\mathrm{MPP}} = 25\,\mathrm{V}$ under STC. The PV curve has been uploaded and updated in the case of solar irradiance changes using Keysight commands through MATLAB. The MPPT algorithms that control the boost have been implemented in MATLAB/Simulink. Then, by using dSPACE real-time interface, the program has been compiled and uploaded to dSPACE 1103 controller board. The MPPT used for providing the references in the case of implementing FMPC-MPPT is the P&O algorithm. The MPPT frequency was set to 25 Hz, with a voltage step size of $\Delta V = 0.25$ V for the voltage reference and a current step size of $\Delta I = 0.01$ A for the current reference. The model of the boost converter used in the simulation model is designed for the grid-connected system, but the one used in the experimental setup is a smaller one (400-W power), with smaller inductor compared to the one used in the simulation model. The ideal operation of this boost converter is at 35-kHz switching frequency, which corresponds approximately to 30-μs switching/sampling period.

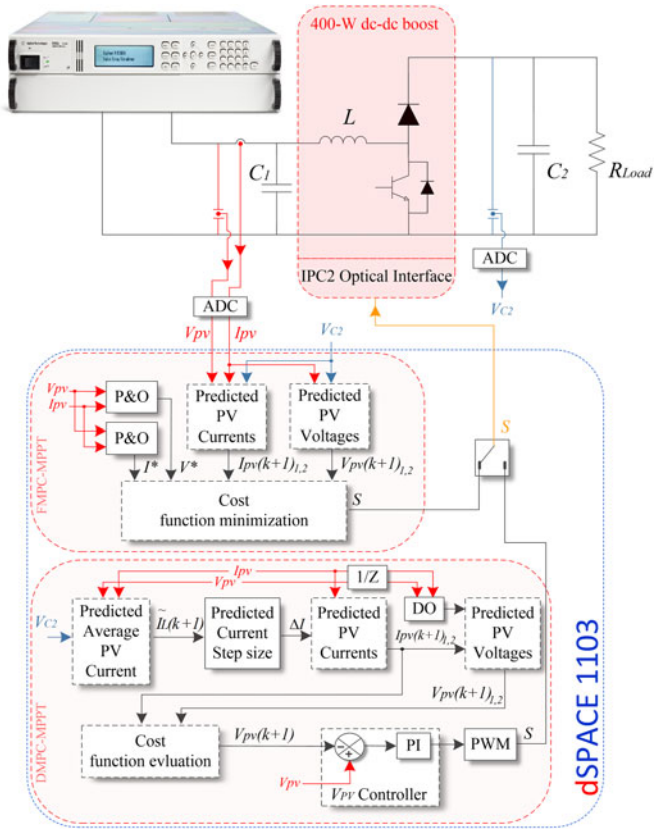

Fig. 12. Global diagram of the experimental test bench and the main control structure of both discrete MPC-MPPT methods using a boost converter.

C. Static Tests According to the EN 50530 Standard

The static tests were done under seven defined solar irradiation levels. In each level, the inverter voltage was set to the minimum MPP voltage (V_{min}), the rated MPP voltage (V_{rtd}), and the maximum MPP voltage (V_{max}). The static efficiency was calculated based on these tests by using the European weighting factors as follows [58]:

$$\eta_{\mathrm{EU}} = 0.03 \cdot \eta_{05\%} + 0.06 \cdot \eta_{10\%} + 0.13 \cdot \eta_{20\%} + 0.10 \cdot \eta_{30\%} + 0.48 \cdot \eta_{50\%} + 0.20 \cdot \eta_{100\%} \tag{32}$$

as well as by California Energy Commission (CEC) weighting factors (33)

$$\eta_{\mathrm{CEC}} = 0.04 \cdot \eta_{10\%} + 0.05 \cdot \eta_{20\%} + 0.12 \cdot \eta_{30\%} + 0.21 \cdot \eta_{50\%} + 0.53 \cdot \eta_{75\%} + 0.05 \cdot \eta_{100\%}. \tag{33}$$

$\eta_{05\%}$ means the efficiency of the MPPT for a PV string working under 5% of the solar irradiation under standard conditions. At each irradiation level, the efficiency was calculated by the following expression:

$$\eta = \frac{1}{P_{\mathrm{av}} \cdot T_M} \sum_{i=1}^{n} P_{\mathrm{pv}} \cdot \Delta T \tag{34}$$

where P_{av} is the available power in the PV string, P_{pv} is the extracted power from the PV string, T_M is the total measurement

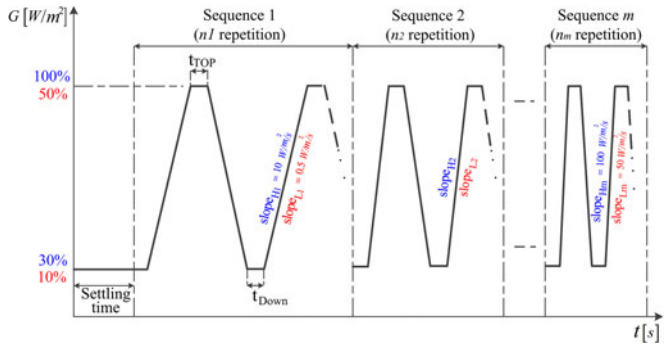

Fig. 13. Irradiance profiles used to calculate the dynamic efficiency of the MPPT, according to the EN 50530 standard. The red and blue colors indicate the solar irradiation ranges and slopes of the very low to medium irradiance test and the low- to high-solar-irradiance test, respectively.

time, ΔT is the sampling period of the efficiency calculation loop, and n is the total number of periods.

D. Dynamic Tests According to the EN 50530 Standard

The dynamic efficiency was calculated by applying to the emulated PV string trapezoidal irradiation profiles executed in two successive tests: a very low to medium test in a range of 10–50% of the solar irradiance under STC and, after a defined settling time, a low- to high-irradiance test in a range of 30–100% of the solar irradiance under STC, as shown in Fig. 13. Each test was done in several defined sequences, and in each sequence, the irradiation profile has been repeated several defined times. The slope in the very low to medium irradiance test was varying from 0.5 W/m^2/s in the first sequence ($slope_{L1}$) up to 50 W/m^2/s in the last sequence ($slope_{Lm}$), whereas the slope in low- to high-irradiance test was varying from 10 W/m^2/s in the first sequence ($slope_{H1}$) up to 100 W/m^2/s in the last sequence ($slope_{Hm}$) [59]. In every separate repetition, the dynamic efficiency was calculated by using the following expression:

$$\eta_{\mathrm{Dyn},i} = \frac{1}{\sum_{j=1}^{n} P_{\mathrm{av}} \cdot \Delta T} \cdot \sum_{j=1}^{n} P_{\mathrm{pv}} \cdot \Delta T. \tag{35}$$

Being n_m the number of repetitions, the dynamic efficiency corresponding to EN50530 standards can be written as

$$\eta_{\mathrm{Dyn}} = \frac{1}{n_m} \sum_{i=1}^{n_m} \eta_{\mathrm{Dyn},i}. \tag{36}$$

The aim of repeating the irradiation profiles in each sequence is not to estimate the average MPPT efficiency. These repetitions are performed to calculate the efficiency of an MPPT integrated into the whole system under test [58]. Based on this, the simulation model was constructed to execute only one irradiation profile per sequence.

E. Model Parameter Mismatch

It is well known that the presence of modeling errors can affect MPC controllers. The mismatch between the real value of the parameter and the value that has been set in the mathematical model causes to a deviated prediction of the controlled variable. This may lead to a wrong decision for the selection of the switching state when reaching a certain threshold of model parameter mismatch. This threshold varies according to the MPC control type and the power converter topology. For this purpose, we have performed several tests using the aforementioned converters. The values of the parameters were adjusted for different mismatch levels in a range of -30% to $+30\%$. Note that these tests have been performed under the STC.

TABLE III
SIMULATION RESULTS OF THE MPPT EFFICIENCY CALCULATED USING THE EUROPEAN FORMULA (%)

Power Converter	Voltage	P&O	FMPC-MPPT	DMPC-MPPT
Boost	V_{MPP}_min	99.81	99.80	99.83
	V_{MPP}_rated	99.95	99.97	99.98
	V_{MPP}_max	99.93	99.96	99.95
	Average	99.89	99.91	99.92
Z-source inverter	V_{MPP}_min	99.92	99.83	99.95
	V_{MPP}_rated	99.91	99.93	99.96
	V_{MPP}_max	99.88	99.95	99.97
	Average	99.90	99.90	99.96
Flyback	V_{MPP}_min	99.92	99.93	99.93
	V_{MPP}_rated	99.92	99.94	99.94
	V_{MPP}_max	99.89	99.91	99.92
	Average	99.91	99.92	99.93

TABLE IV
SIMULATION RESULTS OF THE MPPT EFFICIENCY CALCULATED USING CALIFORNIA'S FORMULA (%)

Power Converter	Voltage	P&O	FMPC-MPPT	DMPC-MPPT
Boost	V_{MPP}_min	99.87	99.87	99.91
	V_{MPP}_rated	99.96	99.98	99.94
	V_{MPP}_max	99.94	99.97	99.96
	Average	99.92	99.94	99.94
Z-source inverter	V_{MPP}_min	99.95	99.91	99.95
	V_{MPP}_rated	99.92	99.93	99.96
	V_{MPP}_max	99.90	99.96	99.96
	Average	99.92	99.93	99.95
Flyback	V_{MPP}_min	99.93	99.94	99.95
	V_{MPP}_rated	99.93	99.95	99.95
	V_{MPP}_max	99.90	99.93	99.94
	Average	99.92	99.94	99.95

V. RESULTS AND DISCUSSION

A. Simulation Results

For comparison purposes, P&O has also been implemented on the same system and tested under the static and dynamic conditions. Tables III and IV show the efficiencies of P&O, FMPC, and DMPC calculated by using both the European and California´s formulas, respectively. Unlike the efficiency of the inverter, the efficiency of the MPPT normally is calculated with a resolution of two decimals [4]. It can be seen from these tables that the efficiencies of these methods are the same in some cases and extremely close in the other cases, with a maximum difference of 0.03%. However, in only one case (η_{Euro} of ZSI),

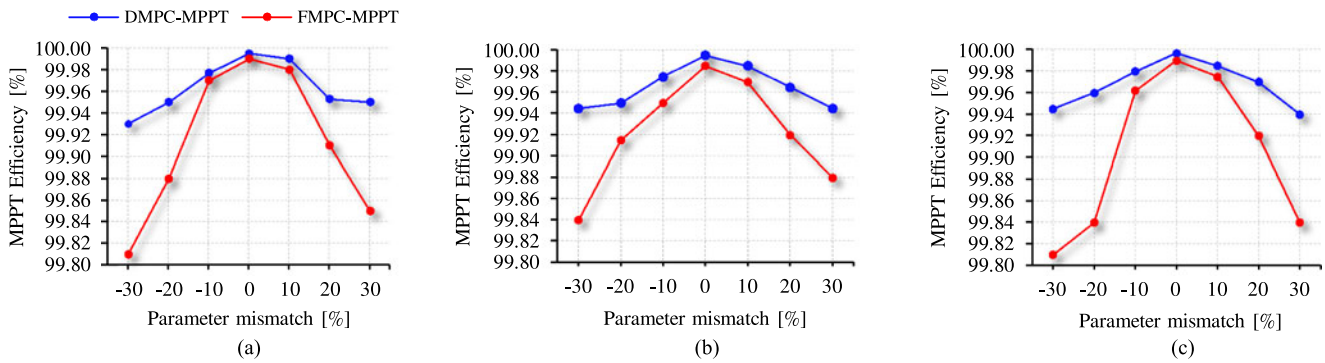

Fig. 14. Simulation results of FMPC-MPPT and DMPC-MPPT efficiencies under STC and in the case of model parameter mismatch using (a) a boost converter "L and C_2," (b) a Z-source inverter "C_1 and L_1," and (c) a flyback converter "C and L_m."

TABLE V
SIMULATION RESULTS OF THE MPPT EFFICIENCIES UNDER EN50530 STANDARD DYNAMIC CONDITIONS (%) AND TIME CONVERGENCE UNDER THE STC (S)

Power Converter	η_{Dyn}			Time Convergence		
	P&O	FMPC-MPPT	DMPC-MPPT	P&O	FMPC-MPPT	DMPC-MPPT
Boost	98.50	98.62	99.18	0.42	0.39	0.27
Z-source inverter	98.11	98.23	99.03	0.36	0.31	0.26
Flyback	98.37	98.48	99.02	0.25	0.26	0.13

TABLE VI
EXPERIMENTAL RESULTS OF THE MPPT EFFICIENCIES UNDER EN50530 STANDARD CONDITIONS USING A BOOST CONVERTER (%)

η	P&O	FMPC-MPPT	DMPC-MPPT
η_{Euro}	99.73	99.76	99.68
η_{CEC}	99.85	99.87	99.79
η_{Dyn}	98.12	98.19	98.57

DMPC shows a relatively better efficiency with a difference of 0.06% compared to other methods.

As can be seen from Table V, there is a clear difference between P&O and DMPC dynamic performances. DMPC has a better dynamic efficiency for all the converters. The minimum difference is 0.65%, which corresponds to the flyback converter, whereas the dynamic efficiency of FMPC is very close to the efficiency of P&O with a maximum difference of 0.12%.

The results shown in Fig. 14(a)–(c) were obtained, where the system was working with model parameter inaccuracy. As observed from these figures, the efficiency of FMPC decreases to 99.80% when the system is working with ±30% model parameter mismatch. DMPC's efficiency decreases to 99.90% when it is working with ±30% parameter mismatch. It can be concluded that FMPC-MPPT is more influenced by the parameter mismatch, whereas DMPC-MPPT shows a robustness for this test. Also, it is worth mentioning that the overestimation of the parameters in all these converters is less influencing than their underestimation.

B. Experimental Results

In order to confirm the results found by the simulation models, experimental tests have been carried out. Table VI summarizes both EN 50530 static and dynamic efficiencies using a boost converter in the case of a standalone system (see Fig. 12). It can be seen from the table that the static efficiencies of FMPC-MPPT are very close to P&O, showing a difference of 0.03% and 0.02% for η_{Euro} and η_{CEC}, respectively, which is still within the statical range between two successive tests. Regarding DMPC-MPPT static efficiencies, they are less than P&O static efficiencies, with a difference of 0.05% and 0.06% for η_{Euro} and η_{CEC}, respectively. However, they are within the agreement of the outdoor results reported in [60].

Also, the difference between the dynamic efficiency of FMPC-MPPT and P&O is within the statical range between two successive tests, whereas there is a significant difference between the dynamic efficiency of DMPC-MPPT and the others. Therefore, some figures of some repetitions of these MPPTs working under EN50530 standard dynamic conditions are presented (see Figs. 15 and 16). These figures correspond to repetitions from the last three sequences.

Again, it can be seen from these figures that FMPC-MPPT has the same behavior as P&O, and FMPC-MPPT fails to pursue the MPP in the same sequences the P&O fails. In Figs. 15(a) and 16(b), FMPC-MPPT first failed, and then, it converged to the MPP. DMPC-MPPT shows a better performance compared to FMPC-MPPT in this test. Actually, it did not fail for pursuing the MPP in all the sequences, except in the last sequence from very low to medium irradiance test [see Fig. 15(c)]. Also, it did not track the MPP well in the last sequence from low to high insolation test [see Fig. 16(c)].

In this paper, only repetitions from the last three sequences from EN 50530 standard dynamic conditions have been presented because P&O and FMPC-MPPT start fail to pursue the MPP in these sequences.

As can be seen from Figs. 15 and 16, DMPC-MPPT operates with a significant oscillation under low irradiance levels; these oscillations are even bigger than the oscillations of P&O. This justifies why the statistical efficiencies of this method are less

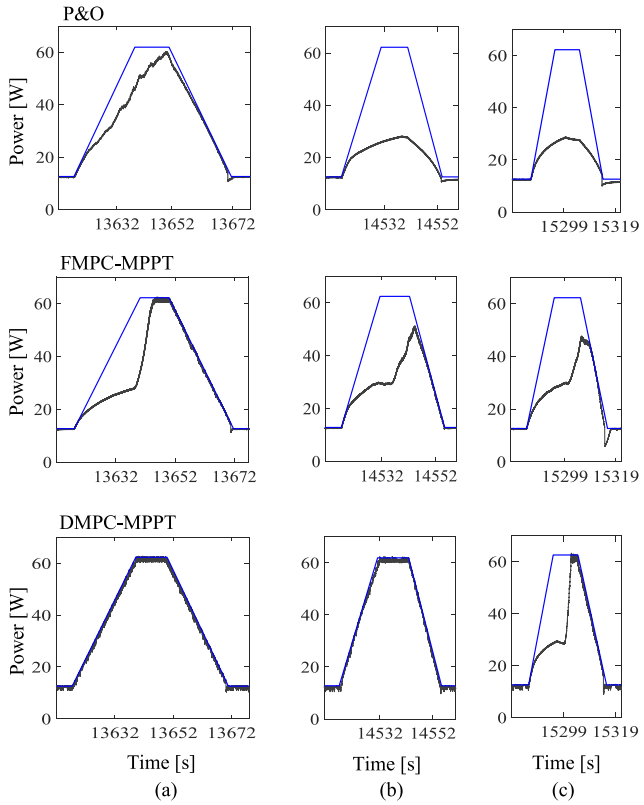

Fig. 15. Experimental results of P&O, FMPC-MPPT, and DMPC-MPPT, respectively, under very low to medium irradiance EN50530 standard test "10–50%." (a) One repetition from the sequence before the last two sequences "20 W/m^2/s." (b) One repetition from the one before the last sequence "30 W/m^2/s." (c) One repetition from the last sequence "50 W/m^2/s."

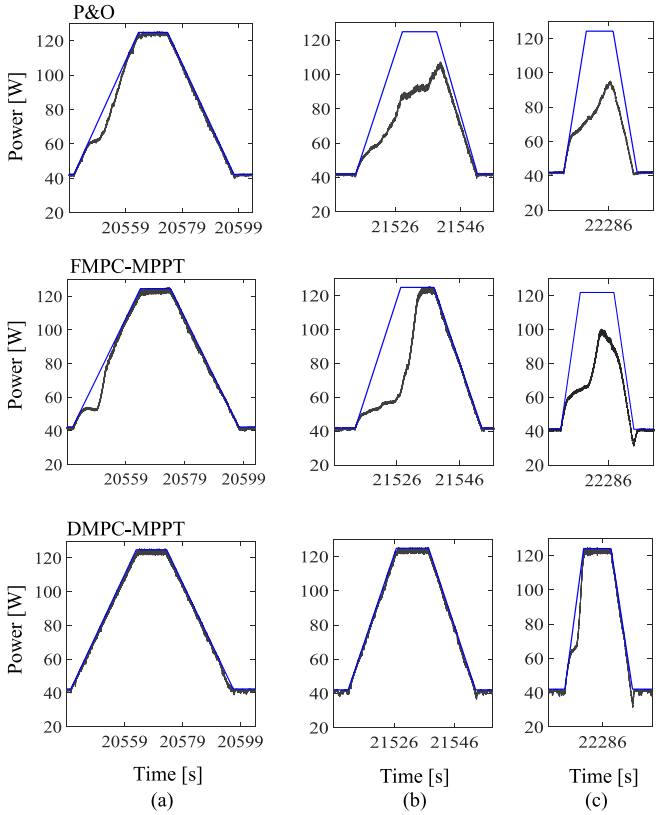

Fig. 16. Experimental results of P&O, FMPC-MPPT, and DMPC-MPPT, respectively, under low- to high-irradiance EN50530 standard test "30–100%." (a) One repetition from the sequence before the last two sequences "30 W/m^2/s." (b) One repetition from the one before the last sequence "50 W/m^2/s." (c) One repetition from the last sequence "100 W/m^2/s."

than the efficiencies of the other methods presented in Table VI. But, from Tables III and IV, the simulation model did not reveal these oscillations. During low insolation levels, the fill form factor decreases, and since the prediction model of DMPC-MPPT is performed based on the PV characteristic, some measurement noise will cause a deviation of the predicted variable out of the PV characteristic.

Fig. 17 shows the experimental results of FMPC-MPPT and DMPC-MPT, where the system was operating under the STC and with model parameter misestimated. This figure shows that the efficiency of FMPC-MPPT decreased to 99.38% when the system was working with −30% model parameter mismatch, whereas DMPC-MPPT decreased to 99.86%. When the parameters of the system were overestimated by 30%, FMPC-MPPT exhibits a decreased efficiency of 99.50%, whereas DMPC-MPPT decreased to 99.87%. Also, It is worth noting that sensitivity to model parameter inaccuracy is asymmetrical. We can conclude from this figure that FMPC-MPPT is again more influenced by the model parameter mismatch, and that, because FMPC-MPPT uses the model of the converter for the decision based on the difference between the references and the predicted variables, DMPC-MPPT uses the converter parameters just for the estimation of the shifting step size.

Table VII shows a summarized comparison of these methods in terms of computational cost, dynamic performance,

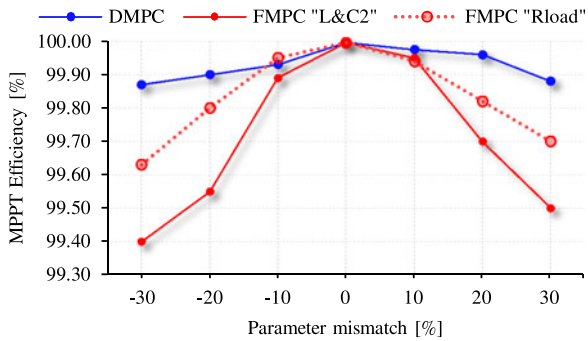

Fig. 17. Experimental results of FMPC-MPPT and DMPC-MPPT efficiencies under STC in the case of model parameter mismatch "L and C_2." The red-dashed line represents FMPC efficiencies with load value misestimated "R_{load}."

oscillation under low insolation levels, and model parameter dependence. During one sample period Ts, the measurement, algorithm execution, and actuation times added all together should fit in. Also, since the gating pulses used to control the converter are generated directly from the control algorithm, the sampling frequency must be greater than or equal to the switching frequency [24]. These two aforementioned conditions are the boundaries that should be taken into account when selecting the sampling frequency. The use of the modulation stage makes the choice of the sampling time when implementing DMPC

TABLE VII
COMPARISON OF DISCRETE MODEL-PREDICTIVE-CONTROL-BASED MPPTS

	Boost			Z-source inverter			Flyback		
	P&O	FMPC	DMPC	P&O	FMPC	DMPC	P&O	FMPC	DMPC
Sampling frequency (Computational cost)	Low	Extremely high	Very high	Low	High	High	Low	Very high	Very high
Processing time	5.58 μs	8.36 μs	8.71 μs	-	-	-	-	-	-
Dynamic performance	Poor	Poor	Above average	Poor	Poor	Average	Poor	Poor	Above average
Oscillation under low insolations	Exist	Exist	Large	Exist	Exist	Large	Exist	Exist	Large
Model parameter dependence	No	High	Exist	No	High	Exist	No	High	Exist

more flexible. Hence, the computation cost is highly dependent on the switching frequency of the converter rather than the used approach.

The processing time has been calculated by using the dSpace Profiler program during the operation of the system, as can be seen from Table VII; the processing time of the conventional P&O is less than the processing time of MPC-MPPTs. On the other hand, the difference between FMPC and DMPC is only 0.35 μs. But, it can be estimated that in the case of a three-phase converter, the difference between these two methods will extend, since the prediction in FMPC is going to be for each phase apart. It is worth noting that the above computation times include the full control algorithm and additional overhead by the dSpace system, not only the MPPT algorithm itself. We also expect that in the case of implementation on a microcontroller with dedicated interrupts for the different control functions, differences in the computational cost between P&O and MPC methods will increase.

VI. CONCLUSION

In FMPC-MPPT, only the behavior of the converter based on its mathematical model is considered for performing the predictions. Since the reference tracked by FMPC is generated by using the P&O/INC algorithm, the oscillation in the output PV power under steady meteorological conditions will be inherited from P&O/INC. Also, under changing atmospheric conditions, the dynamic performance of FMPC-MPPT will be inherited from P&O as well. Hence, the application of FMPC on MPPT does not conquer the problems of the classical MPPTs. Indeed, the application of FMPC on MPPT overcomes the drawbacks of the PI controller used in the voltage control loop of the MPPT (in the case of voltage control).

DMPC-MPPT is less sensitive to model parameter mismatch, and it has a better dynamics compared to FMPC-MPPT during rapid environmental condition changes. However, during low solar irradiance levels (when the PV curve's knee is flatter), and in real application, some noise measurement may lead to an extrapolation with a slope's sign opposite to the PV curve's slope sign. Therefore, the prediction will be in the wrong direction. After running several loops under these circumstances, a relatively high-power oscillation will be produced at the terminals of the PV array.

As a general conclusion, the DMPC-MPPT method is advised for implementation instead of FMPC-MPPT, especially in areas where environmental conditions suddenly change.

REFERENCES

[1] International Energy Agency, World Energy Investment Outlook |Special Report, 2016. [Online]. Available: https://www.iea.org/ newsroom /news/2016/october/iea-raises-its-five-year-renewable-growth-forecast as -2015-marks-record-year.html

[2] International Energy Agency, Technology Roadmap, Solar Photovoltaic Energy 2016 edition, 2016. [Online]. Available: https://www.iea.org/ publications/freepublications/publication/WorldEnergyOutlook2016Exe cutiveSummaryEnglish.pdf

[3] S. Sajadian and R. Ahmadi, "Model predictive-based maximum power point tracking for grid-tied photovoltaic applications using a *Z*-source inverter," *IEEE Trans. Power Electron.*, vol. 31, no. 11, pp. 7611–7619, Nov. 2016.

[4] D. Sera, L. Mathe, T. Kerekes, S. V. Spataru, and R. Teodorescu, "On the perturb-and-observe and incremental conductance MPPT methods for PV systems," *IEEE J. Photovoltaics*, vol. 3, no. 3, pp. 1070–1078, Jul. 2013.

[5] N. Femia, G. Petrone, G. Spagnuolo, and M. Vitelli, "A technique for improving P&O MPPT performances of double-stage grid-connected photovoltaic systems," *IEEE Trans. Ind. Electron.*, vol. 56, no. 11, pp. 4473–4482, Nov. 2009.

[6] M. A. Elgendy, B. Zahawi, and D. Atkinson, "Operating characteristics of the P&O algorithm at high perturbation frequencies for standalone PV systems," *IEEE Trans. Energy Convers.*, vol. 30, no. 1, pp. 189–198, Mar. 2015.

[7] M. B. Shadmand, X. Li, R. S. Balog, and H. A. Rub, "Model predictive control of grid-tied photovoltaic systems: Maximum power point tracking and decoupled power control," in *Proc. 1st Workshop Smart Grid Renewable Energy*, Doha, Qatar, 2015, pp. 1–6.

[8] Y. Mahmoud, M. Abdelwahed, and E. F. El-Saadany, "An enhanced MPPT method combining model-based and heuristic techniques," *IEEE Trans. Sustain. Energy*, vol. 7, no. 2, pp. 576–585, Apr. 2016.

[9] N. Femia, G. Petrone, G. Spagnuolo, and M. Vitelli, "Optimization of perturb and observe maximum power point tracking method," *IEEE Trans. Power Electron.*, vol. 20, no. 4, pp. 963–973, Jul. 2005.

[10] A. Safari and S. Mekhilef, "Simulation and hardware implementation of incremental conductance MPPT with direct control method using cuk converter," *IEEE Trans. Ind. Electron.*, vol. 58, no. 4, pp. 1154–1161, Apr. 2011.

[11] M. A. Elgendy, B. Zahawi, and D. J. Atkinson, "Assessment of the incremental conductance maximum power point tracking algorithm," *IEEE Trans. Sustain. Energy*, vol. 4, no. 1, pp. 108–117, Jan. 2013.

[12] T. K. Soon and S. Mekhilef, "Modified incremental conductance MPPT algorithm to mitigate inaccurate responses under fast-changing solar irradiation level," *Sol. Energy*, vol. 101, pp. 333–342, 2014.

[13] W. Xu, C. Mu, and J. Jin, "Novel linear iteration maximum power point tracking algorithm for photovoltaic power generation," *IEEE Trans. Appl. Supercond.*, vol. 24, no. 5, Oct. 2014, Art. no. 0600806.

[14] B. Subudhi and R. Pradhan, "A comparative study on maximum power point tracking techniques for photovoltaic power systems," *IEEE Trans. Sustain. Energy*, vol. 4, no. 1, pp. 89–98, Jan. 2013.

[15] A. Al Nabulsi and R. Dhaouadi, "Efficiency optimization of a DSP-based standalone PV system using fuzzy logic and dual-MPPT control," *IEEE Trans. Ind. Informat.*, vol. 8, no. 3, pp. 573–584, Aug. 2012.

[16] Syafaruddin, E. Karatepe, and T. Hiyama, "Artificial neural network-polar coordinated fuzzy controller based maximum power point tracking control under partially shaded conditions," *IET Renew. Power Gener.*, vol. 3, no. 2, pp. 239–253, Jul. 2009.

[17] J. Holtz and S. Stadtfeld, "A predictive controller for the stator current vector of AC machines fed from a switched voltage source," in *Proc. Int. Power Electron. Conf.*, 1983.

[18] J. Rodriguez *et al.*, "State of the art of finite control set model predictive control in power electronics," *IEEE Trans. Ind. Informat.*, vol. 9, no. 2, pp. 1003–1016, May 2013.

[19] P. Cortes, A. Wilson, S. Kouro, J. Rodriguez, and H. Abu-Rub, "Model predictive control of multilevel cascaded H-Bridge inverters," *IEEE Trans. Ind. Electron.*, vol. 57, no. 8, pp. 2691–2699, Aug. 2010.

[20] S. Vazquez *et al.*, "Model predictive control: A review of its applications in power electronics," *IEEE Ind. Electron. Mag.*, vol. 8, no. 1, pp. 16–31, Mar. 2014.

[21] M. Aleenejad, H. Mahmoudi, and R. Ahmadi, "A modified space vector modulation method for fault-tolerant operation of multilevel converters," *IEEE Trans. Power Electron.*, 2015.

[22] P. Cortes, M. P. Kazmierkowski, R. M. Kennel, D. E. Quevedo, and J. Rodriguez, "Predictive control in power electronics and drives," *IEEE Trans. Ind. Electron.*, vol. 55, no. 12, pp. 4312–4324, Dec. 2008.

[23] J. Rodríguez and P. Cortes, *Predictive Control of Power Converters and Electrical Drives*, 1st ed. New York, NY, USA: Wiley–IEEE Press, 2012.

[24] R. Errouissi, S. M. Muyeen, A. Al-Durra, and Siyu Leng, "Experimental validation of a robust continuous nonlinear model predictive control based grid-interlinked photovoltaic inverter," *IEEE Trans. Ind. Electron.*, vol, 63, no 7, pp. 4495–4505, Jul. 2016.

[25] R. Erase, S. M. Muyeen, A. Al-Durra, and S. Leng, "A robust continuous-time MPC of a DC–DC boost converter interfaced with a grid-connected photovoltaic system," *IEEE J. Photovoltaics*, vol. 6, no. 6, pp. 1619–1629, Nov. 2016.

[26] M. B. Shadmand, R. S. Balog, and H. Abu-Rub, "Model predictive control of PV sources in a smart DC distribution system: Maximum power point tracking and droop control," *IEEE Trans. Energy Convers.*, vol. 29, no. 4, pp. 913–921, Dec. 2014.

[27] S. Sajadian and R. Ahmadi, "Distributed maximum power point tracking using model predictive control for solar photovoltaic applications," in *Proc. IEEE Appl. Power Electron. Conf. Expo.*, Tampa, FL, USA, 2017, pp. 1319–1325.

[28] R. P. Aguilera and D. E. Quevedo, "On stability and performance of finite control set MPC for power converters," in *Proc. Workshop Predictive Control Electr. Drives Power Electron.*, Munich, Germany, 2011, pp. 55–62.

[29] R. P. Aguilera and D. E. Quevedo, "Predictive control of power converters: Designs with guaranteed performance," *IEEE Trans. Ind. Informat.*, vol. 11, no. 1, pp. 53–63, Feb. 2015.

[30] P. Cortes, J. Rodriguez, C. Silva, and A. Flores, "Delay compensation in model predictive current control of a three-phase inverter," *IEEE Trans. Ind. Electron.*, vol. 59, no. 2, pp. 1323–1325, Feb. 2012.

[31] M. B. Shadmand, M. Mosa, R. S. Balog, and H. A. Rub, "An improved MPPT technique for high gain DC-DC converter using model predictive control for photovoltaic applications," in *Proc. IEEE Appl. Power Electron. Conf. Expo.*, Fort Worth, TX, USA, 2014, pp. 2993–2999.

[32] O. Abdel-Rahim, H. Funato, and J. Haruna, "An efficient MPPT technique with fixed frequency finite-set model predictive control," in *Proc. IEEE Energy Convers. Congr. Expo.*, Montreal, QC, Canada, 2015, pp. 6444–6449.

[33] M. B. Shadmand, M. Mosa, R. S. Balog, and H. A. Rub, "Maximum power point tracking of grid connected photovoltaic system employing model predictive control," in *Proc. IEEE Appl. Power Electron. Conf. Expo.*, Charlotte, NC, USA, 2015, pp. 3067–3074.

[34] P. E. Kakosimos and A. G. Kladas, "Implementation of photovoltaic array MPPT through fixed step predictive control technique," *Renewable Energy*, vol. 36, pp. 2508–2514, 2011.

[35] O. Abdel-Rahim and H. Funato, "Model predictive control based maximum power point tracking technique applied to ultra step-up boost converter for PV applications," in *Proc. IEEE Innovative Smart Grid Technol., Asia*, Kuala Lumpur, Malaysia, 2014, pp. 138–142.

[36] M. Metry, S. Bayhan, R. S. Balog, and H. Abu Rub, "Model predictive control for PV maximum power point tracking of single-phase sub multilevel inverter," in *Proc. Power Energy Conf., Illinois*, Feb. 2016, pp. 1–8.

[37] A. A. Abushaiba, S. M. M. Eshtaiwi, and R. Ahmadi, "A new model predictive based maximum power point tracking method for photovoltaic applications," in *Proc. IEEE Int. Conf. Electro Inf. Technol.*, Grand Forks, ND, USA, 2016, pp. 571–575.

[38] P. E. Kakosimos, A. G. Kladas, and S. N. Manias, "Fast photovoltaic-system voltage- or current-oriented MPPT employing a predictive digital current-controlled converter," *IEEE Trans. Ind. Electron.*, vol. 60, no. 12, pp. 5673–5685, Dec. 2013.

[39] R. Kadri, J. P. Gaubert, and G. Champenois, "An improved maximum power point tracking for photovoltaic grid-connected inverter based on voltage-oriented control," *IEEE Trans. Ind. Electron.*, vol. 58, no. 1, pp. 66–75, Jan. 2011.

[40] M. E. Ropp and S Gonzalez, "Development of a MATLAB/Simulink model of a single phase grid-connected photovoltaic system," *IEEE Trans. Energy Convers.*, vol. 24, no. 1, pp. 195–202, Mar. 2009.

[41] A. Bakeer, M. A. Ismeil, and M. Orabi, "A powerful finite control set-model predictive control algorithm for quasi Z-source inverter," *IEEE Trans. Ind. Informat.*, vol. 12, no. 4, pp. 1371–1379, Aug. 2016.

[42] M. Metry, M. B. Shadmand, R. S. Balog, and H. Abu-Rub, "MPPT of photovoltaic systems using sensorless current-based model predictive control," *IEEE Trans. Ind. Appl.*, vol. 53, no. 2, pp. 1157–1167, Apr. 2017.

[43] K. Ishaque, Z. Salamb, and G. Laussc, "The performance of perturb and observe and incremental conductance maximum power point tracking method under dynamic weather conditions," *Elsevier Trans. Appl. Energy*, vol. 119, pp. 228–236, Apr. 2014.

[44] D. Sera, R. Teodorescu, J. Hantschel, and M. Knoll, "Optimized maximum power point tracker for fast-changing environmental conditions," *IEEE Trans. Ind. Electron.*, vol. 55, no. 7, pp. 2629–2637, Jul. 2008.

[45] M. Mosa, H. Abu Rub, M. E. Ahmed, and J. Rodríguez, "Modified MPPT with using model predictive control for multilevel boost converter," in *Proc. 38th Annu. Conf. IEEE Ind. Electron. Soc.*, Montreal, QC, Canada, 2012, pp. 5080–5085.

[46] M. A. Morales-Caporal, J. D. J. Rangel-Magdaleno, J. M. Ramirez-Cortes, E. Tlelo-Cuatle, and R. Morales-Caporal, "Control algorithm using trajectory-based MPC for MPPT application," in *Proc. IEEE Int. Autumn Meeting Power, Electron. Comput.*, 2015, Ixtapa, Mexico, pp. 1–6.

[47] O. Lopez-Lapena, M. T. Penella, and M. Gasulla, "A closed-loop maximum power point tracker for subwatt photovoltaic panels," *IEEE Trans. Ind. Electron.*, vol. 59, no. 3, pp. 1588–1596, Mar. 2012.

[48] O. Abdel-Rahim and H. Funato, "An experimental investigation of modified predictive hysteresis control based MPPT strategy for PV applications," in *Proc. IEEE Energy Convers. Congr. Expo.*, Montreal, QC, Canada, 2015, pp. 6450–6454.

[49] Y. Yang and F. Blaabjerg, "A modified P&O MPPT algorithm for single-phase PV systems based on deadbeat control," in *Proc. 6th IET Int. Conf. Power Electron., Machines Drives*, Bristol, U.K., 2012, pp. 1–5.

[50] S. Kouro, P. Cortes, R. Vargas, U. Ammann, and J. Rodriguez, "Model predictive control-a simple and powerful method to control power converters," *IEEE Trans. Ind. Electron.*, vol. 56, no. 6, pp. 1826–1838, Jun. 2009.

[51] T. Geyer, G. Papafotiou, and M. Morari, "Model predictive direct torque control—Part I: Concept, algorithm, and analysis," *IEEE Trans. Ind. Electron.*, vol. 56, no. 6, pp. 1894–1905, Jun. 2009.

[52] G. Papafotiou, J. Kley, K. G. Papadopoulos, P. Bohren, and M. Morari, "Model predictive direct torque control—Part II: Implementation and experimental evaluation," *IEEE Trans. Ind. Electron.*, vol. 56, no. 6, pp. 1906–1915, Jun. 2009.

[53] P. Fang Zheng, "Z-source inverter," *IEEE Trans. Ind. Appl.*, vol. 39, no. 2, pp. 504–510, Mar./Apr. 2003.

[54] S. Miaosen, W. Jin, A. Joseph, P. Fang Zheng, L. M. Tolbert, and D. J. Adams, "Constant boost control of the Z-source inverter to minimize current ripple and voltage stress," *IEEE Trans. Ind. Appl.*, vol. 42, no. 3, pp. 770–778, May/Jun. 2006.

[55] S. Miaosen, W. Jin, A. Joseph, F. Z. Peng, L. M. Tolbert, and D. J. Adams, "Maximum constant boost control of the Z-source inverter," in *Proc. IEEE Ind. Appl. Conf.*, 2004, p. 147.

[56] O. Machado, P. Martin Sanchez, F. J. Rodriguez, and E. Bueno, "A neural network-based dynamic cost function for the implementation of a predictive current controller," *IEEE Trans. Ind. Informat.*, 2017, to be published.

[57] S. Sajadian and R. Ahmadi, "Distributed maximum power point tracking using model predictive control for photovoltaic energy harvesting architectures based on cascaded power optimizers," *IEEE J. Photovoltaics*, vol. 7, no. 3, pp. 849–857, May 2017.

[58] R. Bründlinger, N. Henze, H. Häberlin, B. Burger, A. Bergmann, and F. Baumgartner, "prEN 50530—The New European Standard for performance characterisation of PV inverters," in *Proc. 24th Eur. Photovoltaic Sol. Energy Conf.*, Hamburg, Germany, Sep. 2009, pp. 3105–3109.

[59] H. Häberlin, "New test procedure for measuring dynamic MPP tracking efficiency at grid connected PV inverters," in *Proc. 24th Eur. Photovoltaic Sol. Energy Conf.*, Hamburg, Germany, Sep. 2009, pp. 3631–3637.

[60] S. B. Kjaer, "Evaluation of the 'hill climbing' and the 'incremental conductance' maximum power point trackers for photovoltaic power systems," *IEEE Trans. Energy. Convers.*, vol. 27, no. 4, pp. 922–929, Dec. 2012.

Abderezak Lashab (S'13) received the bachelor's and master's degrees in electrical engineering in 2010 and 2012, respectively, from Université des Frères Mentouri Constantine, Constantine, Algeria, where he is currently working toward the Ph.D. degree with the Department of Electrical Engineering.

His current research interests include control, modeling, and diagnostics of photovoltaic power systems, and power electronics.

Dezso Sera (S'05–M'08–SM'15) received the B.Sc. and M.Sc. degrees in electrical engineering from the Technical University of Cluj-Napoca, Cluj-Napoca, Romania, in 2001 and 2002, respectively, the M.Sc. degree in power electronics and the Ph.D. degree in photovoltaic systems from the Department of Energy Technology, Aalborg University, Aalborg, Denmark, where he is currently an Associate Professor.

Since 2009, he has been a Program Leader of the Photovoltaic Systems Research Program (www.pv-systems.et.aau.dk) with the Department of Energy Technology, Aalborg University. His research interests include modeling, characterization, diagnostics, and maximum power point tracking of photovoltaic (PV) arrays, as well as power electronics and grid integration for PV systems.

Josep M. Guerrero (S'01–M'04–SM'08–F'15) received the B.S. degree in telecommunications engineering, the M.S. degree in electronics engineering, and the Ph.D. degree in power electronics from the Technical University of Catalonia, Barcelona, Spain, in 1997, 2000, and 2003, respectively.

Since 2011, he has been a Full Professor with the Department of Energy Technology, Aalborg University, Aalborg, Denmark, where he is responsible for the Microgrid Research Program (www.microgrids.et.aau.dk). His research interests are oriented to different microgrid aspects, including power electronics, distributed energy-storage systems, hierarchical and cooperative control, energy management systems, smart metering, and the Internet of Things for ac/dc microgrid clusters and islanded minigrids, and recently especially focused on maritime microgrids for electrical ships, vessels, ferries, and seaports.

Prof. Guerrero is an Associate Editor for the IEEE TRANSACTIONS ON POWER ELECTRONICS, the IEEE TRANSACTIONS ON INDUSTRIAL ELECTRONICS, and the IEEE INDUSTRIAL ELECTRONICS MAGAZINE, and an Editor for the IEEE TRANSACTIONS ON SMART GRID.

Laszlo Mathe received the B.Sc. degree in electrical engineering and the M.Sc. degree from the Technical University of Cluj-Napoca, Cluj-Napoca, Romania, in 2000 and 2002, respectively, and the Ph.D. degree in electrical engineering from the Department of Energy Technology, Aalborg University, Aalborg, Denmark, in 2010.

Between 2002 and 2007, he was a Control Development Engineer. He is currently an Associate Professor with Aalborg University. His current research interests include control and design of power converters, control of electrical drives, photovoltaic systems, modulation techniques (modular multilevel converters and two-level inverters), and vehicle electrification.

Aissa Bouzid received the Ph.D. degree in electrical engineering from Paris 6 University, Paris, France, in 1992.

He is currently the Dean of the Faculty of Engineering, Université des Frères Mentouri, Constantine, Algeria, where he is also a Full Professor with the Department of Electrical Engineering. His current research interests include control, modeling, and diagnostics of both photovoltaic and wind power systems, and power electronics.